J Mater Sci (2011) 46:2518–2528
DOI 10.1007/s10853-010-5102-3

Laser annealing of neutron irradiated boron-10 isotope doped diamond

K. Jagannadham · M. J. Lance · J. E. Butler

Received: 19 August 2010 / Accepted: 20 November 2010 / Published online: 14 December 2010

Abstract ^{10}B isotope doped p-type diamond epilayer grown by chemical vapor deposition on (110) oriented type IIa diamond single crystal substrate was subjected to neutron transmutation at a fluence of 2.4×10^{20} thermal and 2.4×10^{20} fast neutrons. After neutron irradiation, the epilayer and the diamond substrate were laser annealed using Nd–YAG laser irradiation with wave length, 266 nm and energy, 150 mJ per pulse. The neutron irradiated diamond epilayer and the substrate were characterized before and after laser annealing using different techniques. The characterization techniques include optical microscopy, secondary ion mass spectrometry, X-ray diffraction, Raman, photoluminescence and Fourier Transform Infrared spectroscopy, and electrical sheet conductance measurement. The results indicate that the structure of the irradiation induced amorphous epilayer changes to disordered graphite upon laser annealing. The irradiated substrate retains the (110) crystalline structure with neutron irradiation induced defects.

Introduction

Neutron irradiation of diamond has been investigated to determine the effects of the radiation damage in type Ia,b and type IIa [1–8] and type IIb crystals [9–12]. More recently, neutron transmutation of ^{10}B isotope to ^{7}Li ions has been attempted to achieve n-type electrical conductivity starting from p-type diamond [10–12]. Previous experiments indicated that n-type activity could be achieved after irradiation for 400 h in a thermal flux of 10^{12} neutrons/cm^2 s [12]. Compensation of p-type B with n-type Li has been observed in the electrical conductance. However, there is an ongoing debate on the origin of n-type activity in the p-type B doped diamond that has been subject to transmutation. Radiation induced defects and complexes are also known to give rise to n-type activity [13–15]. More recently, deuterium complex with B [16, 17] was shown to exhibit n-type conductivity that is stable up to only 200 °C.

Fast neutrons with higher energy (>1 MeV) give rise to lattice damage by displacement of carbon atoms as the scattering cross-section is higher (1.6 barns). Thermal neutrons (<0.1 eV) do not give rise to any significant lattice damage because the scattering cross-section is lower (0.001 barns) and it is estimated that the threshold for carbon atom displacement is between 20 and 30 eV [10–12]. However, irradiation with thermal neutron flux is accompanied by radiation damage from the transmutation reaction that gives out high energy (1.0 MeV) Li^+ ions and (1.78 MeV) He^+ ions or alpha-particles. It should be noted that the scattering cross-section of thermal neutrons with ^{10}B is much higher (3837 barns) than that of fast neutrons (0.1 barns). These charged particles of Li^+ and He^+ undergo electronic scattering initially and nuclear scattering in the final stages. The electronic scattering does not contribute to the lattice damage. The damage from nuclear scattering in the form of displacement of carbon atoms and Li^+ ions is retained in the diamond lattice. Li^+ ions are known to occupy interstitial sites [18–20]. While the

K. Jagannadham (✉)
Materials Science and Engineering, North Carolina State University, Raleigh, NC 27695, USA
e-mail: jag_kasichainula@ncsu.edu

M. J. Lance
High Temperature Materials Laboratory, Oak Ridge National Laboratory, Oak Ridge, TN 27831-6068, USA

J. E. Butler
Code 6174, Naval Research Laboratory, Washington, DC 20375, USA

electrical conductivity from thermally doped Li in diamond has been found to increase [20], there is still a question if it contributes to n-type conductivity. Lattice damage is also responsible for generation of point defects and complexes [10–12] and amorphization of the diamond.

Thermal annealing at 1000 °C for 8 h after neutron irradiation of ^{10}B doped diamond to a fluence of 2.66×10^{20} thermal neutrons/cm^2 and 3.14×10^{20} fast neutrons/cm^2 has been used to study the changes in electrical conductivity and lattice perfection [10, 11]. Although, the electrical conductance of the neutron irradiated diamond was higher with activation energy of 0.37 eV characteristic of p-type B, the result after thermal annealing was a large reduction in conductance with an activation energy of 0.20 eV characteristic of either Li or radiation induced defects [10, 11].

It has been known in semiconductors [21] and diamond [22, 23] that implantation damage can be recovered by laser annealing leading to solid phase epitaxial growth with the presence of active dopants. In the present work, we have carried out laser annealing of the neutron irradiated ^{10}B doped diamond to determine the changes in the lattice structure and the properties. We have performed characterization of the diamond epilayer and the substrate by different methods.

Experimental results

^{10}B isotope doped diamond epilayer of thickness 4 μm was grown by chemical vapor deposition on polished type IIa diamond substrate of size 4 mm × 4 mm × 0.3 mm. The B dopant concentration was 10^{19} at. cm^{-3}. The epilayer and the diamond substrate were subjected to neutron irradiation in a thermal flux of 10^{14} n/cm^2 sec and an equal fast neutron flux for 4 weeks in a high flux reactor. The temperature of the sample during or immediately after irradiation was not monitored. The fluence of both the thermal or fast neutrons in the sample is 2.42×10^{20} n/cm^2. The epilayer and the substrate were characterized prior to and after irradiation. X-ray diffraction showed that the epilayer was (110) oriented and it followed that of the substrate. The sample consisting of the neutron irradiated epilayer and the diamond substrate was laser annealed using Nd–YAG laser irradiation on the epilayer surface for 15 s using the wave length of 266 nm, pulse repetition of 10 Hz, pulse duration 8–9 ns, laser fluence of 150 mJ per pulse and beam diameter 0.8 cm. It should be mentioned that the sample was held in front of a graphite block with a fine tweezers so that the transmitted laser beam was absorbed by the graphite. It was found that a fraction of the laser beam was transmitted. Also, the sample cross-section was only 0.16 cm^2 whereas that of the laser beam was 0.5 cm^2. Thus, approximately only a third of the laser energy was incident on the epilayer surface.

Optical microscopy and secondary ion mass spectrometry of the epilayer

Optical microscope image of the epilayer after irradiation followed by laser annealing is presented in Fig. 1. The surface of the unirradiated epilayer was smooth although the roughness was not recorded. Several intersecting (111) surface traces at 70.5° were observed on the epilayer surface after irradiation and laser annealing of the epilayer. These crack configurations were found after neutron irradiation of the epilayer and the substrate, but before the laser anneal. The results of secondary ion mass spectrometry (SIMS) are presented in our earlier work [12] and showed $^7Li/^{10}B$ atom ratio slightly above 2 in the epilayer after irradiation. There was a decrease in the Li concentration very close to the surface but reached the full value within a depth of 0.2 to 0.3 μm from the surface of the epilayer. These results have not changed after laser annealing and therefore the SIMS depth profile is not repeated here. SIMS maps for ^7Li and ^{10}B have also shown that the distribution of the two elements is uniform in the film [12].

X-ray diffraction

X-ray diffraction of the epilayer and the substrate mounted on Si(001) wafer was carried out using Phillips X'PERT PRO MRD HR instrument using Cu K_α ($\lambda = 0.15405$ nm) radiation. X-ray diffraction of the sample before laser annealing showed that the epilayer is amorphous and the substrate retained the crystalline lattice with (110) preferred orientation [12]. Results of X-ray diffraction of the sample performed after annealing are shown in Fig. 2. The sample was mounted on Si(100) oriented wafer using

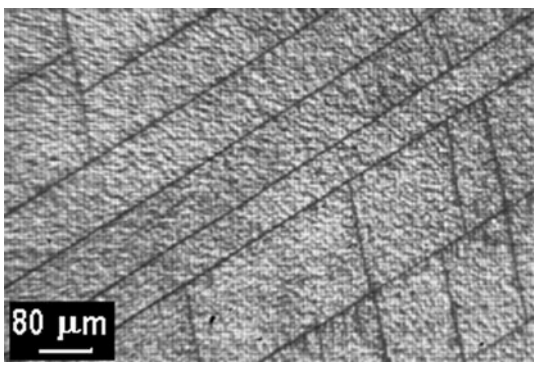

Fig. 1 Optical micrograph of the epilayer after neutron irradiation and laser annealing showing surface traces of intersecting cracks at 70.5°

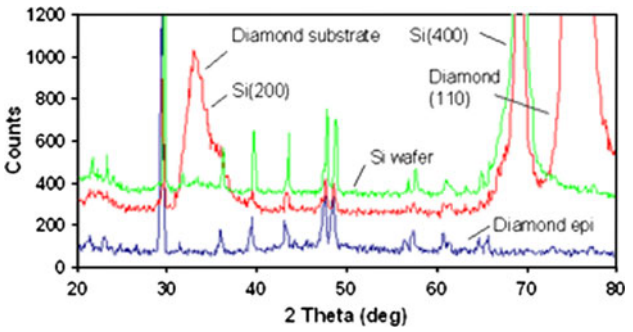

Fig. 2 Grazing incidence X-ray diffraction from epilayer on diamond placed on Si with clay, normal diffraction (θ–2θ) from irradiated diamond substrate side on Si wafer with clay, and normal diffraction from Si wafer and clay without diamond

plastic clay for performing the normal and grazing incidence X-ray diffraction. The peak patterns in Fig. 2 are labeled to indicate the different layers examined. The pattern labeled "diamond substrate" was obtained with normal incidence (θ–2θ) and shows the peaks from (110) irradiated diamond substrate, Si(400) and the Si(200) forbidden reflection. The Si(200) forbidden peak at $2\theta = 33°$ is known to arise from double diffraction and its intensity is found to increase when the wafer is aligned well for the (400) peak. The other peaks in this pattern are identified to arise from the mounting clay, which was determined by measuring the X-ray diffraction pattern from a Si wafer with mounting clay on it. The resulting pattern is labeled "Si wafer" in Fig. 2. The absence of the Si(200) forbidden peak is not surprising as the alignment of the wafer could be slightly away from the (400) orientation. Based on the control experiments, we find the pattern of the irradiated diamond substrate has only one peak associated with (110) diamond. To determine if the epilayer recovered its crystalline structure after laser annealing, the grazing incidence (at 1° incidence) was recorded and it is labeled "diamond epi". This pattern contained no other peaks than those associated with the mounting clay present around the sample and therefore it is concluded that the epilayer after irradiation and annealing shows no evidence of crystallinity. If the epilayer consists of nanocrystalline regions, there could be weak and broad peaks that were not identified in the grazing incidence pattern due to low count time.

Raman spectroscopy

Confocal Raman spectroscopy was performed using Horiba Jobin–Yvon Lab Ram Aramis microRaman spectrometer with spatial resolution of 0.6 cm^{-1}. Raman spectrum of diamond epilayer deposited by chemical vapor deposition contains the first order phonon peak at 1332 cm^{-1}, as shown in Fig. 3a. The presence of a strong Fano interference in the diamond Raman peak that is associated with

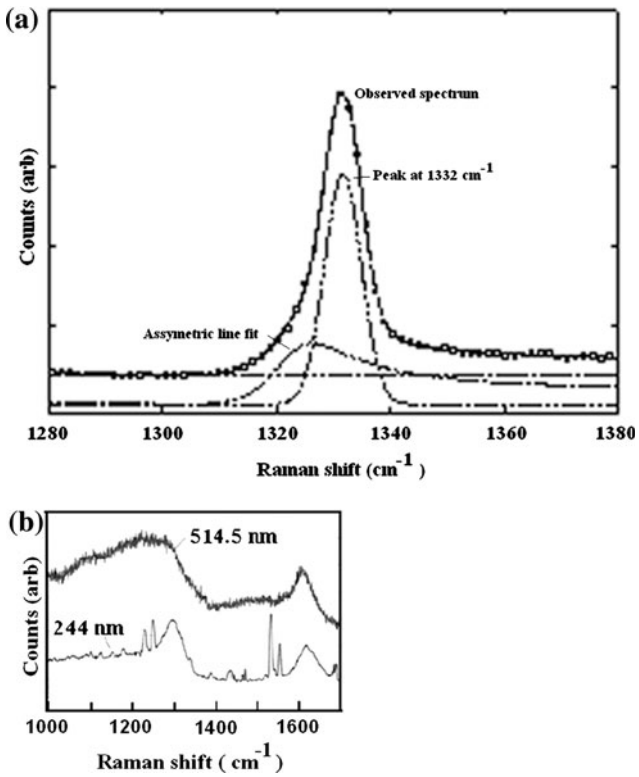

Fig. 3 **a** Raman spectrum of as grown epilayer of diamond collected using 514.5 nm laser excitation. A strong Fano interference associated with high boron dopant concentration and characteristic diamond peak at 1332 cm^{-1} are present. The Raman data points were fitted using a Voigt peak and an asymmetric line fit described by the Fano line shape. The two fitting functions are *dashed lines* and the final fit is the *solid line* connecting the data points. **b** Raman spectra of heavily irradiated diamond observed using 514.5 and 244 nm laser excitation

high B concentration (10^{19} at. cm^{-3}) is clearly seen when the observed spectrum is resolved into the symmetric and asymmetric parts. Raman spectrum of the epilayer [12] after irradiation is presented in Fig. 3b that shows the changes that took place upon irradiation. The broad background in the region between 1000 and 1400 cm^{-1} obtained using 514.5 nm laser excitation indicates that the film is amorphous or highly defective. A broad peak was observed at 1614 cm^{-1} that is characteristic of the glassy carbon. This peak is shifted to a lower value from 1631 cm^{-1}, a peak observed in ion implanted diamond with 4 MeV carbon atoms [24] or in diamond implanted with 3.5 MeV He ions [25]. The spectrum obtained using the 244 nm laser excitation contains the details of the broad peak in the one phonon region. Also, peaks are present at 1530 and 1550 cm^{-1} in addition to the peak associated with glassy carbon at 1614 cm^{-1}. These sharp peaks except the peak at 1614 cm^{-1} are thought to be artifacts from the laser plasma, although other peaks were observed previously in diamond films subjected to heavy ion-implantation

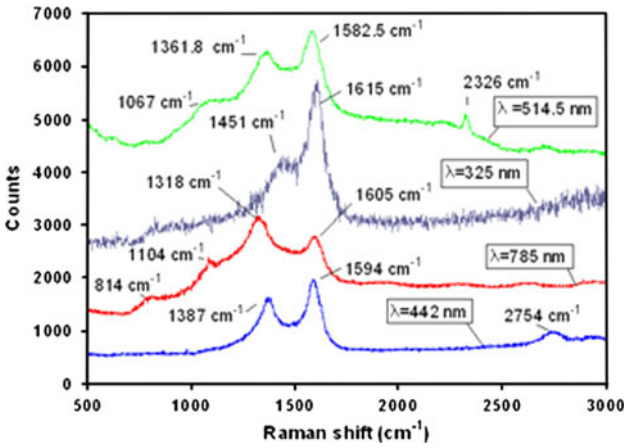

Fig. 4 Raman spectra of annealed epilayer observed using four laser wave lengths

damage [24, 25]. It should be noted that although a peak close to 1300 cm^{-1} is observed, there are no peaks at 1360 and 1580 cm^{-1} that are associated with nanocrystalline or disordered graphite.

Raman spectrum of the laser annealed epilayer was observed using different wave lengths of laser excitation and presented in Fig. 4. The spectra are characterized by two major peaks called the "D peak" at 1350 cm^{-1} that arises from disordered regions and the "G peak" at 1580 cm^{-1} that arises from nanocrystalline graphite [26–30]. The changes in the selection rules for Raman active phonon modes scattered by disordered regions that are normally inactive in the infinite lattice of graphite give rise to the "D peak". Dispersion in Raman modes as a result of double resonance in Raman scattering [31] is responsible for the shift in the peak positions with excitation wave length. Both the Lorentzian fitted peak positions and the intensity ratio of the D peak to the G peak (I_D/I_G) are functions of the size of the nanocrystalline regions [26, 28, 31] present in the film. The ratio of the intensity of the peaks has been correlated using the results obtained with 514.5 nm laser excitation [26, 28, 31] and the crystallite size is estimated to be 6.4 nm. This ratio I_D/I_G decreased with increase in the incident photon energy. The position of the D peak is shown in Fig. 5 as a function of laser photon energy. A similar variation of the G peak was observed after deconvolution and fitting with Lorentz peak shapes. A second order D peak or 2D peak was observed at 2755 and 2700 cm^{-1} in the spectra obtained with 442 and 514.5 nm laser excitation, respectively, as seen in Fig. 4.

Raman spectroscopy images of the epilayer were observed using 532 nm laser excitation. The observed Raman spectrum is shown in Fig. 6 with the D peak at 1347 cm^{-1} and G peak at 1588 cm^{-1} and the corresponding second order peaks at 2700 and 2943 cm^{-1}, respectively. A Raman intensity map was obtained from

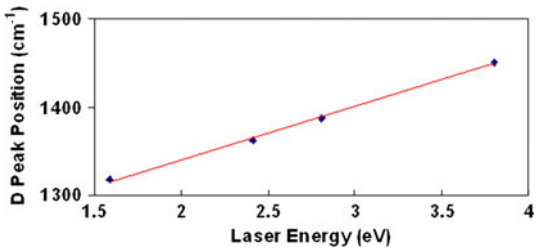

Fig. 5 Position of the D peak from the epilayer with change in the incident photon energy

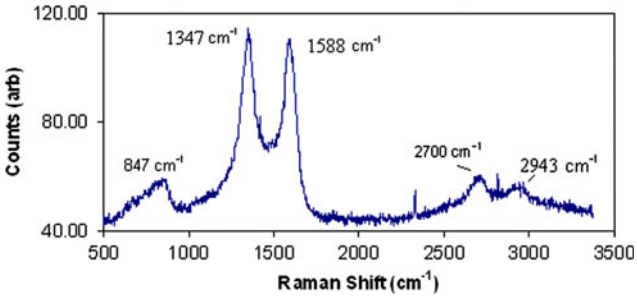

Fig. 6 Raman spectrum of the epilayer observed using 530 nm laser excitation. The peaks at 1347 and 1588 cm^{-1} are used to create the images of the epilayer that are shown in Figs. 7 and 8, respectively

an area of 25 μm × 25 μm from the center using the 1347 cm^{-1} peak. Figure 7a is an optical image from a larger area of the epilayer surface on which the Raman intensity map from the center is superimposed. The magnified Raman intensity map for 1347 cm^{-1} peak from the 25 μm × 25 μm area is also shown in Fig. 7b. The region with the highest intensity of the 1347 cm^{-1} peak is approximately 8 μm in diameter and shown in black (red). Thus, the area shown in black (red) is the region which is strongly contributing to the peak at 1347 cm^{-1}. A similar Raman intensity map was obtained from an area of 25 μm × 25 μm from the center using the 1588 cm^{-1} peak. Figure 8a is an optical image from a larger area of the epilayer surface on which the Raman intensity map for the 1588 cm^{-1} peak is superimposed. The magnified Raman intensity map of the 1588 cm^{-1} peak from the 25 μm × 25 μm area is shown in Fig. 8b. Thus, the area shown in black (red) is the region which is strongly contributing to the peak at 1588 cm^{-1}.These two regions of the 1347 and 1588 cm^{-1} peak maps are nearly from the same area. The adjacent regions shown in different colors in both the images have significantly less Raman intensity, as described in the figure legends. These images show that two small, ca. 8 μm regions are the main contributors to the Raman intensity at 1347 cm^{-1} and 1588 cm^{-1}.

Raman spectra of the type IIa irradiated diamond substrate observed using different wave lengths of laser excitation are shown in Fig. 9. The results followed the previously observed spectrum with defect induced diamond

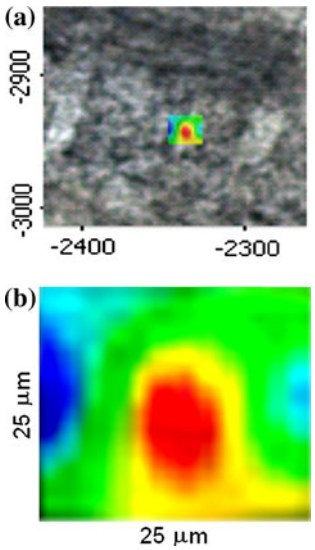

Fig. 7 **a** An optical image of a larger area of the epilayer surface. The Raman intensity map (see **b**) collected from a square area of 25 µm × 25 µm is superimposed on the optical image of the epilayer surface at the center. The dimensions are shown in micrometers. **b** The Raman intensity map of the 1347 cm^{-1} peak collected using 530 nm laser excitation from the 25 µm × 25 µm area shown in **a** is shown at higher magnification. The region shown in *black at the center* (*red*) has the highest intensity and the region shown in *black at the left* (*blue*) has the lowest intensity of the 1347 cm^{-1} peak with the other colors showing the dimensions of the regions with decreasing intensity. The *horizontal* and *vertical axes* are 25 µm each (Color figure online)

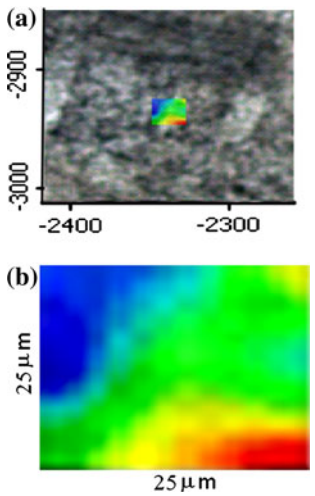

Fig. 8 **a** An optical image of a larger area of the epilayer surface. Raman intensity map of the 1588 cm^{-1} peak (see **b**) collected from a square area of 25 µm × 25 µm is superimposed on the optical image of the epilayer surface at the center. The dimensions are shown in micrometers. **b** The Raman intensity map of the 1588 cm^{-1} peak collected using 530 nm laser excitation from the 25 µm × 25 µm area shown in **a** is shown at higher magnification. The region shown in *black at the bottom right* (*red*) has the highest intensity and the region shown in *black at the left* (*blue*) has the lowest intensity of the 1588 cm^{-1} peak with the other colors showing the dimensions of the regions with decreasing intensity. The *horizontal* and *vertical axes* are 25 µm each (Color figure online)

peak appearing close to 1316 cm^{-1} for laser excitation wave length of 532 nm [24, 25]. The ratio of the intensity of the diamond peak at 1316 cm^{-1} to that at 1631 cm^{-1} was determined. This ratio increased when lower photon energy or higher wave length of the laser excitation was used.

Photoluminescence (PL) spectroscopy

PL was carried out at room temperature with the same instrument used for the Raman spectroscopy. PL spectra from the irradiated epilayer before and after laser annealing were obtained using 514.5 nm laser excitation and are shown in Fig. 10. In addition to the Raman peaks above 2.05 eV, a broad peak centered around 1.88 eV (660 nm) was observed [32–34]. The nitrogen and vacancy complex related peaks at 1.945 eV or 637 nm ($N–V^-$), 2.154 eV or 575 nm (N–V) and 2.46 eV or 504 nm (N–V–N) were not observed. The GR1 band associated with V° defects previously observed at low levels of neutron irradiation [12] was also absent.

PL spectra of the irradiated diamond substrate and the epilayer were observed using laser excitation wave length at 442 nm and shown in Fig. 11. The range of this spectrum does not cover the 1.88 eV peak. However, a broad peak near 2.35 eV was observed.

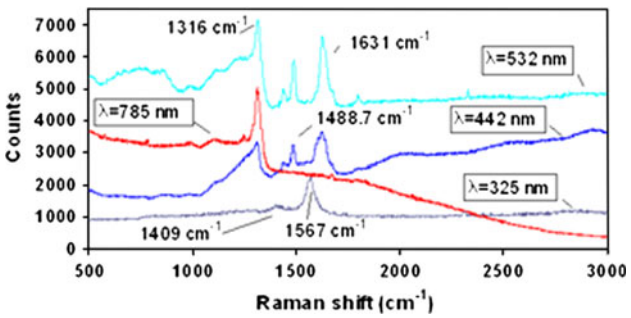

Fig. 9 Raman spectra of irradiated diamond substrate obtained using different laser wave length excitation

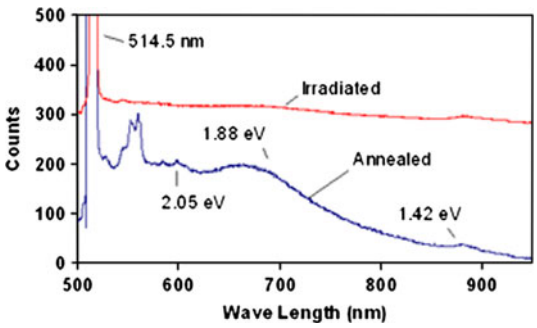

Fig. 10 PL spectra of the irradiated and laser annealed epilayer taken using 514.5 nm laser wave length excitation

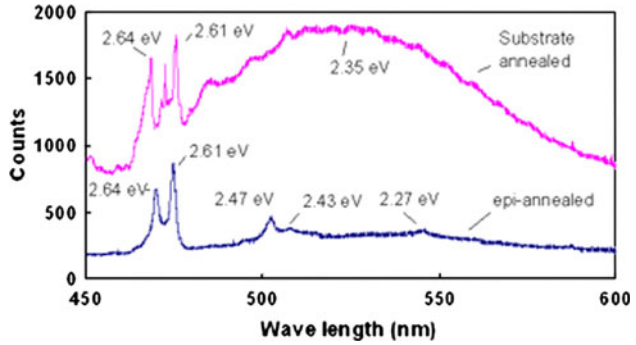

Fig. 11 PL spectra of the laser annealed epilayer and irradiated diamond substrate taken using 442 nm laser wave length excitation

Fourier transform infrared (FTIR) spectroscopy

FTIR spectrum of the epilayer and the substrate was collected using Thermo Electron Nicolet 8700 spectrometer with resolution of 0.01 cm^{-1}. The infrared absorption spectrum of the annealed epilayer and that of the ^{10}B doped unirradiated epilayer are shown in Fig. 12. The spectrum was very noisy between 1085 and 1250 cm^{-1} due to the low level of the transmitted light and the detector saturation. The increase in absorption between 1100 and 1332 cm^{-1} is associated with ^{10}B dopant atoms and defects present from irradiation. The peaks associated with B at 780 and 1010 cm^{-1} were also observed. However, peaks that arise from interstitials and complexes, usually observed in neutron irradiated samples at lower fluence [6–9, 12, 35, 36] at 1420, 1530, 1570, and 1910 cm^{-1}, were absent as a result of high strain and disordered graphite structure. An improvement in the transmittance above 1332 cm^{-1} was observed after laser annealing as shown in Fig. 13. This result indicates improvement in crystallinity and reduction in defects and strain upon annealing.

The absorption spectrum of the type IIa irradiated diamond substrate was less noisy as shown in Fig. 14. Three characteristic first order phonon peaks; transverse acoustic phonon energy at 0.098 eV (TA), the longitudinal acoustic

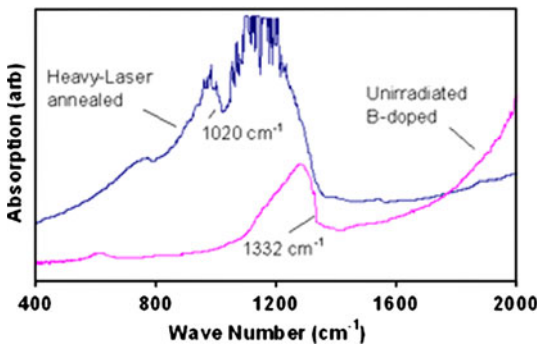

Fig. 12 FTIR absorption spectrum of laser annealed epilayer and ^{10}B isotope doped unirradiated diamond

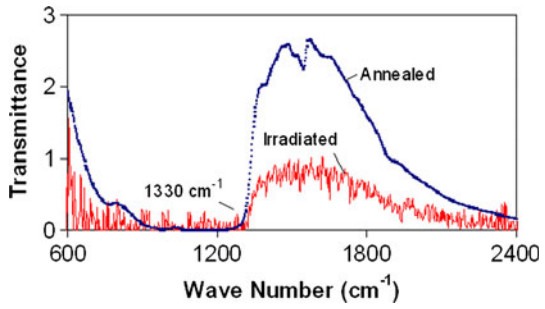

Fig. 13 FTIR transmittance spectrum of laser annealed epilayer and ^{10}B isotope doped unirradiated diamond

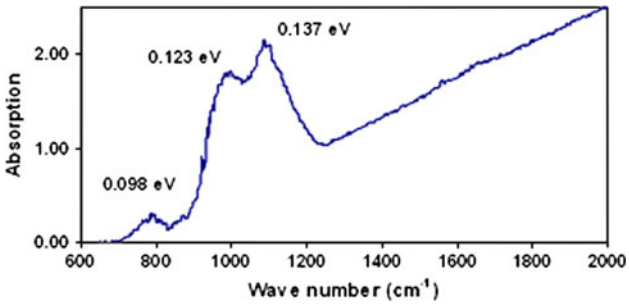

Fig. 14 FTIR spectrum type IIa irradiated diamond substrate

phonon energy at 0.123 eV (LA), and the longitudinal optical phonon energy at 0.137 eV and close to 0.144 eV [35, 36] were observed.

Electrical conductance

Electrical sheet conductance of the epilayer was determined using van der Pauw configuration before and after neutron irradiation and after laser annealing. The sheet conductance of unirradiated diamond epilayer was 56 ohm^{-1}. The temperature dependence of conductance is shown in Fig. 15a with an activation energy of 0.30 eV associated with boron. The high resistance of irradiated diamond necessitated use of electrometers for measurement of resistance. The temperature of the sample was controlled to ±0.1°. The sheet conductance of the irradiated sample, shown in Fig. 15b, varied from 1 to 0.01 $(megaohms)^{-1}$ in the temperature range between 500 and 200 K, respectively. The single linear variation gave activation energy of 0.155 eV. The electrical conductance of the annealed sample, shown in Fig. 15b, remained between 0.014 and 0.011 ohm^{-1} in the temperature range between 500 and 200 K, respectively. The temperature dependence of the resistance followed two straight lines with different slopes that gave activation energy of 0.007 eV between 400 and 500 K and 0.0018 eV between 210 and 260 K. Hall mobility measurements were inconclusive on the nature of carriers.

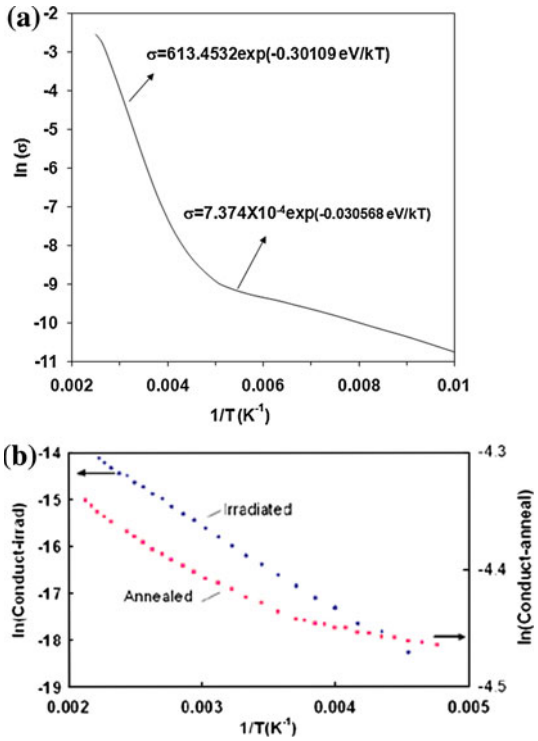

Fig. 15 **a** Electrical sheet conductance in ohm^{-1}, ln(conductance), of as grown epilayer shown as function of temperature (1/*T*). **b** Electrical sheet conductance in ohm^{-1}, ln(conductance), of epilayer after neutron irradiation and after annealing shown as function of temperature (1/*T*)

A comparison of the sheet conductance of the annealed epilayer and the type IIa substrate is presented in Fig. 16. The sheet conductance of the substrate changed between 0.27 and 0.22 (k-ohms)$^{-1}$ in the temperature range between 500 and 200 K, respectively. The variation followed two straight lines with activation energy of 0.008 eV between 400 and 500 K and 0.0018 eV between 210 and 260 K.

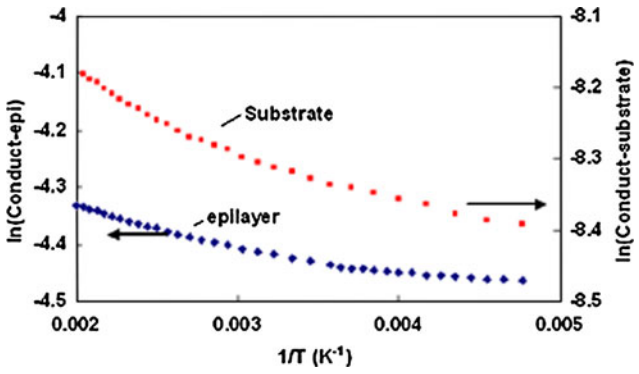

Fig. 16 Electrical sheet conductance in ohm^{-1}, ln(conductance), of type IIa irradiated diamond substrate and epilayer after annealing shown as function of temperature (1/*T*)

Discussion

The intersecting traces on the surface, shown in Fig. 1, were observed after neutron irradiation and these are found to be cracks along (111) planes in the substrate generated by stresses due to the neutron irradiation.

Grazing incidence X-ray diffraction has clearly indicated that the epilayer did not show evidence of crystallinity, whereas the type IIa irradiated substrate is still crystalline. This result indicates that damage created by combined transmutation and fast neutron damage is more severe than that from fast neutrons only.

Raman spectrum of the epilayer, presented in Fig. 4, is similar to that of B implanted graphite annealed at 950 °C [28]. Therefore, the laser annealed epilayer consists of disordered sp^3 arrangement and nanocrystalline regions of graphite. The presence of peaks close to 2720 and 2943 cm^{-1} has also been associated with disorder in the lattice [27]. The shift in the position of the peaks and the changes in intensity are a result of break down of conservation of energy and momentum in scattering due to lack of long range order [31, 33]. Raman spectroscopic images using 532 nm laser excitation and the disorder peak at 1347 cm^{-1} and graphite peak at 1588 cm^{-1} have shown that the regions responsible for these peaks are strong only in a fraction of the area of the film mapped, as shown in Figs. 7b and 8b, respectively.

It is useful to compare the present results with those obtained previously by Khasawinah et. al [10, 11] where neutron irradiation of a ^{10}B doped polycrystalline diamond film on Si followed by thermal annealing at 1000 °C for 8 h which showed a recovery of the diamond peak at 1333 cm^{-1}. Also, X-ray diffraction of the thermal annealed diamond film [10] exhibited the diamond diffraction peaks. In the present work the grazing incidence X-ray diffraction did not reveal any diamond diffraction peaks from the laser annealed epilayer. The Raman spectrum of the unirradiated polycrystalline diamond film on Si used by Khasawinah et al [10, 11] contains a broad peak at 1500 cm^{-1} in addition to the presence of fluorescence background and the absence of a strong Fano interference in the diamond Raman peak that is associated with high B concentrations. In contrast, the epilayer used in the present work was single crystalline before the neutron irradiation and the Raman spectrum of the unirradiated film showed strong Fano interference associated with B concentration of 7.92×10^{19} at.cm^{-3}. These differences are thought to be responsible for a more severe neutron transmutation damage of the epilayer compared to that in the polycrystalline diamond film in the previous work [10, 11].

Pulsed laser annealing of 4 MeV phosphorus implanted diamond to a dose of 10^{15} cm^{-2} where the heavily damaged implant layer is deeply incased in the diamond also

showed regrowth [23, 37, 38]. It was pointed out that diamond regrowth is favored in the presence of deep implants wherein the diamond surface is undamaged and provides a cap layer that constrains the laser heated layer under pressure to convert the damaged carbon layer back to crystalline diamond. It is also shown that graphite always forms in the absence of a surface-constraining diamond layer, for example, in laser etching of diamond surface layers [38]. Thus, combinations of pressure and temperature impact the ability of laser annealing to reform diamond.

It was modeled and found [37] that the temperature reaches 3970 to 5200 K for laser pulse density between 10 and 23 J/cm^2 per pulse. Also, below 10 J/cm^2 per pulse, no visible effects are observed on diamond surface [38]. The laser energy density used in the present experiments is 150 mJ per pulse with the diameter of the circular beam 0.8 cm and circular area 0.5 cm^2 so that the energy density is 0.300 J/cm^2 pulse. We have calculated the temperature increase of the diamond epilayer by assuming all the laser energy in one pulse is absorbed by the epilayer. The specific heat capacity (0.509 J/gm deg) and density (3.5 gm/cm^3) and volume of the epilayer are used in the calculation. The temperature of the epilayer at the end of one pulse (8–9 ns) could not have reached a value higher than 420° above room temperature if there is no thermal conduction. However, dissipation of thermal energy created by the laser irradiation is expected from the higher thermal conductivity of irradiated diamond substrate. The increase in temperature was only 6° after one laser pulse or 60° after 1 s when both the epilayer and diamond substrate of thickness 0.03 cm are included in the evaluation of the temperature. The temperature increase after 15 s of laser irradiation will be 900° without convection and radiation losses. A simple calculation of radiation losses indicated that the temperature at 900 °C will be reduced by 400° per second assuming blackbody radiation. We expect the highest temperature attained to be much lower and near 400 °C. Also, we have not observed any discoloration after laser irradiation.

Graphite formation is not complete in the epilayer as only nanocrystalline graphite is formed. It is possible that the thin epilayer (4 μm) was heated and quenched during laser annealing which is a nonequilibrium process that has not allowed enough time for carbon atom arrangement into the fully graphitic structure or regrowth into diamond from the substrate. The type IIa irradiated diamond substrate with high thermal conductivity is expected to dissipate the heat in the epilayer and the resulting rapid cooling may be responsible for the formation of disordered carbon with nanocrystalline regions. Diamond-like carbon film thermally annealed at moderate temperatures up to 400 °C resulted in only disordered graphite [39]. Thus, the tendency of diamond-like carbon is to form disordered graphite upon low temperature annealing.

The type IIa irradiated diamond substrate was not damaged as much as the epilayer because the transmutation reaction is not present and the ^{7}Li and the He$^+$ ions are mostly confined to the epilayer. However, damage from fast neutrons was responsible for the defects created in the diamond substrate. The X-ray diffraction peak of the (110) strong reflection was retained. The Raman spectrum closely agreed with the pattern that was previously observed in ion beam damaged diamond with 1 MeV and higher energy carbon ions [24] and more closely with that of the defective diamond obtained by 3.5 MeV He$^+$ ions [25]. The Raman peaks previously observed at 1316, 1422, 1447, 1490, 1631, and 1683 cm^{-1} are observed in the spectrum of the irradiated diamond substrate. It has been pointed out that the structure of irradiated diamond consists of nanocrystalline disordered regions created by ion irradiation dispersed in the diamond matrix [25]. Type IIa diamond irradiated below 624 °C with fast neutrons to higher fluence between 1.3×10^{21} and 2.7×10^{21} cm^{-2} also showed [40] Raman spectra similar to that shown in Fig. 9. These results indicate that the substrate contains high density of defects.

PL spectra of the annealed epilayer and the substrate showed broad peaks at 1.88 and 2.35 eV, respectively [32–35]. These peaks are previously observed in diamond powder compacts that are sintered. The diamond compacts contained nitrogen and hence formation of N–V complexes and strain associated with defects was significant. Luminescence from disordered carbon is associated with these broad peaks. The nanocrystalline grain size, high vacancy concentration and strain are found to be responsible for these broad peaks. The peak at 1.85 eV is observed when the particle size is much smaller or when the samples are annealed at high pressure and high temperature [34]. The 2.35 eV peak was observed in annealed diamond but becomes weak in diamond subjected to higher pressure [32–35]. There is no nitrogen in the present diamond sample and therefore we do not associate the peaks with N–V complexes. The GR1 peak from V° vacancies is absent as a result of high concentration of defects. The GR1 peak intensity is found to decrease for higher neutron fluence [12].

The infrared transmission of the diamond epilayer has increased significantly between 1330^{-1} and 2000 cm^{-1} upon annealing, which indicates that the defect density has decreased. All other characteristic peaks associated with interstitials and complexes are absent as the lattice consists of disordered sp^3 carbon and nanocrystalline graphite. Three of the infrared peaks in irradiated substrate are present except the TO peak at 0.159 eV and the LO peak at 0.148 eV. These peaks are associated with defect or

impurity activated peaks in neutron irradiated diamond. These phonon modes are active only in the presence of defects [35, 36]. The absence of the 0.159 eV peak is explained [35] by its proximity to the Raman mode at 0.165 eV. The LO mode at 0.144 and 0.137 eV are interdependent [35] and the first of these two becomes weaker when the second gets stronger [35, 36, 41, 42].

An increase in the electrical resistance was observed previously upon thermal annealing of neutron irradiated diamond [10, 11] that was subjected to transmutation, although recovery of the characteristic Raman peak at 1333 cm^{-1} was present in those samples. In contrast, the electrical resistance of the amorphous epilayer decreased upon laser annealing in the present work. This difference could only be attributed to two different lattice structures that resulted upon laser or thermal annealing. Thermal annealing of neutron irradiated or ion implanted diamond below 1400 °C results in improved Raman spectrum and diamond with fewer defects. On the other hand, laser annealing is responsible for disordered graphite or graphite unless the diamond film is kept under a constraining cap of undamaged diamond [22, 23, 38].

A significant difference in the electrical conductivity (σ) of the irradiated epilayer was observed before and after the laser annealing. We will first consider the neutron irradiated epilayer. The irradiated diamond, although highly resistive, showed an activation energy of 0.155 eV which is much lower than that of B dopant (0.30 eV). This low activation energy is associated either with Li or the defects created during irradiation [10–15, 19, 20]. Electrical conductance of diamond samples implanted with Li at room temperature and without annealing has been found [43] to exhibit very low activation energy (0.02–0.04 eV) but higher conductance than the irradiated epilayer in the present work. However, the resistance of the Li implanted diamond increased upon annealing and the activation energy also increased [43] with both values close to that observed in the present neutron irradiated epilayer. These results suggest that there are two different sources of charge carriers that are activated depending on the temperature during implantation. In the samples implanted at room temperature, the activation energy is lower (0.02–0.4 eV) and the conductance is high. The activation energy is higher (0.19–0.24 eV) when the implantation is performed at higher temperature (850 °C). It has been shown [12] that the temperature of the epilayer has increased during neutron irradiation as a result of the energy transfer from transmutation reaction. Therefore, the electrical conductance of the neutron irradiated epilayer in the present work is similar to that of the higher temperature Li implanted diamond [43]. While this result does not provide direct evidence that the conductance in irradiated sample is from Li dopant, it is obtained only in samples that are either neutron irradiated to achieve Li or Li implanted at higher temperature.

Next, we consider the conductance of the laser annealed epilayer. The resistance of the laser annealed epilayer is low with two activation energy values of 0.007 and 0.0018 eV in different temperature ranges. The conductance is known to exhibit a variable range hoping behavior of carriers if the structure consists of nanocrystalline conducting graphitic regions distributed in insulating amorphous carbon. A similar variation of conductance is observed in diamond-like carbon annealed thermally below 400 °C. Electrical conductance (σ) of diamond-like carbon [44] film in the as deposited and annealed below 400 °C showed the characteristic dependence where $\ln(\sigma)$ is proportional to $T^{1/4}$. When annealed above 600 °C, the dependence on temperature changed to $T^{1/2}$. Based on this, it is concluded that variable range hoping below 400 °C and charge-energy limited tunneling above 400 °C are the active mechanisms of conduction [45]. The electrical conductance of the annealed epilayer and the substrate are replotted against $T^{1/4}$ in Fig. 17 to examine if variable range hoping is active in the epilayer. It is seen that the relation between $\ln(\sigma)$ and $T^{1/4}$ is much closer to linearity than the $1/T$ dependence shown in Fig. 15. The two regions with different slopes are still present. Based on these results, it is thought that variable range hoping is active both in the film and the substrate. The two regions with different slopes may arise from different sources of carriers such as different types of defects or dopants.

The electrical conductance of the neutron irradiated diamond substrate is similar to that of the low temperature ion implanted diamond [43, 46] although the activation energy values are closer to the values determined in the epilayer. In addition, two regions with different slopes are observed. These results suggest that conductance may be associated with the defects that are common to the different structures created either by fast neutron irradiation or ion implantation.

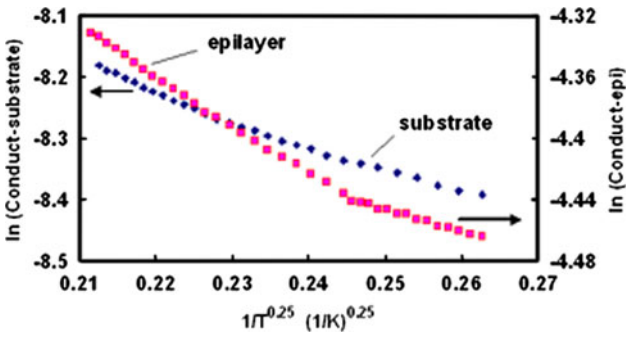

Fig. 17 Electrical sheet conductance in ohm^{-1}, ln(conductance), of type IIa irradiated diamond substrate and epilayer after annealing shown as function of temperature ($1/T^{0.25}$)

Summary and conclusions

^{10}B isotope doped epilayer grown on type IIa diamond substrate was subjected to transmutation reaction with 2.4×10^{20} n/cm^2 thermal and 2.4×10^{20} n/cm^2 fast neutron fluence and subsequent laser annealing using Nd–YAG laser (wavelength of 266 nm) irradiation. Different characterization methods were used to characterize the irradiated and laser annealed epilayer and the diamond substrate. Results showed that the epilayer is converted to disordered graphite containing nanocrystalline graphite regions separated by disordered carbon. The irradiated diamond substrate with high defect density retained crystallinity with (110) preferred orientation. The following important results were obtained through the characterization.

1. Grazing incidence X-ray diffraction of laser annealed diamond epilayer showed no crystalline peaks. Strong (110) peak is obtained from the irradiated diamond substrate.
2. The D and the G peaks were observed in the Raman spectra from the annealed epilayer. The ratio of the intensity of the peaks is used to determine the size of nanocrystalline graphite to be close to 6.4 nm. The peaks associated with irradiated diamond substrate were close to those expected from irradiated diamond with 4 MeV energy ions.
3. Infrared transmittance is improved upon annealing the epilayer. The optical and acoustic phonon peaks that are activated in the presence of defects were observed in the FTIR spectrum associated with the irradiated diamond substrate.
4. Electrical conductance of the neutron irradiated epilayer was closer to that of high temperature Li implanted diamond with activation energy of 0.155 eV.
5. Electrical conductance of laser annealed irradiated epilayer was higher compared to that of the unannealed irradiated epilayer. The temperature dependence could be described by variable range hoping of carriers, however, with two different slopes.
6. Electrical conductance of the irradiated diamond substrate was lower than that of the epilayer. The temperature dependence is similar to that of the ion beam irradiated diamond with variable range hoping of carriers.
7. Neutron irradiated epilayer of boron doped diamond transformed into nanocrystalline graphite dispersed in disordered carbon upon laser annealing.

The results indicate that the structure of the irradiation induced amorphous epilayer changes to disordered graphite upon laser annealing. The irradiated substrate retains the (110) crystalline structure with neutron irradiation induced defects.

Acknowledgements This research is sponsored by the Assistant Secretary for Energy Efficiency and Renewable Energy, Office of Transportation Technologies, as part of the High Temperature Materials Laboratory User Program, ORNL, managed by UT-Battelle, LLC, for the U. S. Department of Energy under contract number DE-AC05-000R22725. SIMS calibration standards were prepared by ion implantation of known concentrations of B and Li. Ion implantation was provided by the Surface Modification and Characterization Research Center at ORNL. JEB acknowledges the support from NRL/ONR. The authors are thankful to Dr. Mark Walters for help in the use of facilities at SMIF, Duke University. The authors are also thankful to Mr. Joseph Dorsheimer of Thermo Scientific for carrying out the Raman spectroscopy imaging of the diamond epilayer surface.

References

1. Levy PW, Kamerer OF (1955) Phys Rev 100:1787
2. Pringsheim P (1953) Phys Rev 91:551
3. Griffiths JHE, Owen J, Ward IM (1955) Magnetic resonance in irradiated diamond and quartz. Proc. Phys. Soc, Defects in crystalline solids, p 81
4. Vance ER (1971) J Phys C: Solid State Phys 4:257
5. Collins AT, Woods GS (1982) Philos Mag B46:77
6. Woods GS (1984) Philos Mag B50:673
7. Clark CD, Ditchburn RW, Dyer HB (1959) Proc Roy Soc Lond A237:75
8. Walker J (1977) J Phys C Solid State Phys 10:3867
9. Clark CD, Ditchburn RW, Dyer HB (1956) Proc Roy Soc Lond 234:363
10. Khasawinah SA, Popovici G, Farmer J, Sung T, Prelas MA, Chamberlain J, White H (1995) J Mater Res 10:2523
11. Popovici G, Melnikov AA, Varichenko VS, Khasawinah SA, Sung T, Prelas MA, Denisenko AB, Penina NM, Martinovitch VA, Drozdova EN, Zaitsev AM, Fahrner WR, Farmer JW, White H, Chamberlain J (1996) Diamond Relat Mater 5:761
12. Jagannadham K, Reed ML, Lance MJ, Watkins TR, Verghese K, Butler JE, Smirnov A (2007) Diamond Relat Mater 16:50
13. Prins JF (1992) Mater Sci Rep 7:271
14. Palmer DW (1994) Properties and growth of diamond, Ed. G. Davies, EMIS, Datareviews Series No.9. INSPEC, London, UK
15. Reznik A, Uzan-Saguy C, Kalish R (2000) Diamond Relat Mater 9:1051
16. Saguy C, Kalish R, Cytermann C, Teukam Z, Chevallier J, Jomard F, Tromson-Carli C, Butler JE, Baron C, Deneuville C (2004) Diamond Relat Mater 13:700
17. Pinault MA, Barjon J, Kociniewski T, Jomard F, Chevallier J (2007) Phys B 401–402:51
18. Prawer S, Saguy CU, Braumstein G, Kalish R (1993) Appl Phys Lett 63:2502
19. Kajihara SA, Antonelli A, Bernholc J, Car R (1991) Phys Rev Lett 66:2010
20. Buckley-Golder IM, Bullough R, Haynes MR, Willis JR, Piller RC, Blamires NG, Gard G, Stephen J (1991) Diamond Relat Mater 1:43
21. Poate JM, Mayer JW (1982) Laser annealing of semiconductors. Academic Press, New York
22. Prawer S, Jamieson DN, Walker RJ, Lee KK, Kalish R (1996) Diamond Films Technol 6:351
23. Allen MG, Prawer S, Jamieson DN, Kalish R (1993) Appl Phys Lett 63:2062

24. Hunn JD, Withrow SP, White CW, Hembree DM Jr (1995) Phys Rev 52B:8106
25. Prawer S, Nugent KW, Jamieson DN (1998) Diamond Relat Mater 7:106
26. Tuinstra F, Koenig JL (1970) J Chem Phys 53:1126
27. Nemanich RJ, Solin SA (1979) Phys Rev 20B:392
28. Elman BS, Dresselhaus MS, Dresselhaus G, Maby EW, Mazurek H (1981) Phys Rev 24B:1027
29. Lespade P, Al-Jishi R, Dresselhaus M (1982) Carbon 20:427
30. Dillon RO, Woollam JA, Katkanant V (1984) Phys Rev 29B:3482
31. Pimenta MA, Dresselhaus G, Dresselhaus MS, Cancado LG, Jorio A, Saito R (2007) Phys Chem Chem Phys 9:1276
32. Evans T, Davey ST, Robertson SH (1984) J Mater Sci 19:2405. doi:10.1007/BF01058119
33. Bergman L, Nemanich R (1997) Handbook of optical properties, vol II. CRC Press, Boca Raton, p 331
34. Webb SW, Jackson WE (1995) J Mater Res 10:1700
35. Smith SD, Hardy JR (1960) Philos Mag 5:1311
36. Smith SD, Taylor W (1962) Proc Phys Soc 79:1142
37. Prawer S, Jamieson DN, Kalish R (1992) Phys Rev Lett 69:2991
38. Liu B, Sandhu GS, Parikh NR, Swanson ML, Chu WK (1990) Nucl Instrum Methods Phys Res, Sect B B45:420
39. Takai K, Oga M, Sato H, Enoki T, Ohki Y, Taomoto A, Suenaga K, Iijima S (2002) Mater Res Symp Proc 699:347
40. Blank VD, Aksenenkov VV, Popov MYU, Perfilov SA, Kulnitskiy BA, YeV Tatyanin, Zhigalina OM, Marvin BN, Denisov VN, Ivlev AN, Chernov VM, Stepanov VA (1999) Diamond Relat Mater 8:1285
41. Gheeraert E, Deneuville A, Mambou J (1998) Diamond Relat Mater 7:1509
42. Hardy JR, Smith SD (1961) Philos Mag 6:1163
43. Job R, Werner M, Denisenko A, Zaitsev A, Fahrner WR (1996) Diamond Relat Mater 5:757
44. Takai K, Oga M, Sato H, Enoki T, Ohki Y, Taomoto A, Suenaga K, Iijima S (2003) Phys Rev 67B:2142021
45. Fung AWP, Rao AM, Kuriyama K, Dresselhaus MS, Dresselhaus G, Endo M, Shindo N (1993) J Mater Res 8:489
46. Prawer S, Kalish R (1995) Phys Rev 51B:15711